

# Stability of aqueous silica nanoparticle dispersions

Cigdem O. Metin · Larry W. Lake ·  
Caetano R. Miranda · Quoc P. Nguyen

Received: 12 April 2010/Accepted: 5 September 2010/Published online: 17 September 2010  
© Springer Science+Business Media B.V. 2010

**Abstract** In this study, we present quantification methods for nanoparticle stability analysis using non-intrusive analytical techniques: attenuated total reflectance, Fourier transform infrared (ATR-FTIR) spectroscopy, ultraviolet-visible (UV-vis) spectrophotometer, zeta potential analyses, and dynamic light scattering (DLS). We use these techniques to study the stability of silica nanoparticle dispersions and the effects of pH, temperature, and electrolytes that would be encountered in oil field brines in a reservoir. Spectral analysis of the Si–O bond at wavenumber of  $1110\text{ cm}^{-1}$  with the ATR-FTIR indicates a structural change on the surface of silica particles as the dispersion pH changes, which agrees with zeta potential measurements. We define a critical salt concentration (CSC) for different salts,

$\text{NaCl}$ ,  $\text{CaCl}_2$ ,  $\text{BaCl}_2$ , and  $\text{MgCl}_2$ , above which the silica dispersion becomes unstable. Three distinct stages of aggregation occur in the presence of salt: clear dispersed, turbid, and separated phases. Divalent cations  $\text{Mg}^{2+}$ ,  $\text{Ca}^{2+}$ , and  $\text{Ba}^{2+}$  are more effective in destabilizing silica nanoparticle dispersion than the monovalent cation  $\text{Na}^+$ . The CSC for  $\text{Na}^+$  is about 100 times more than for  $\text{Ca}^{2+}$ ,  $\text{Ba}^{2+}$ , and  $\text{Mg}^{2+}$ . Among the divalent cations studied,  $\text{Mg}^{2+}$  is the most effective in destabilizing the silica particles. The CSC is independent of silica concentration, and lowers at high temperature.

**Keywords** Silica nanoparticles · Aqueous stability · pH · Temperature · Electrolytes · Aggregation

---

C. O. Metin · L. W. Lake · Q. P. Nguyen (✉)  
Petroleum and Geosystems Engineering Department,  
The University of Texas, 1 University Station, C0300,  
Austin, TX 78712-1061, USA  
e-mail: quoc\_p\_nguyen@mail.utexas.edu

C. O. Metin  
e-mail: cigdem@mail.utexas.edu

L. W. Lake  
e-mail: larry\_lake@mail.utexas.edu

C. R. Miranda  
Universidade Federal do ABC (UFABC)—Centro de  
Ciências Naturais e Humanas, Rua Santa Adélia 166,  
Santo André, SP CEP 09210-170, Brazil  
e-mail: caetano.miranda@ufabc.edu.br

## Introduction

In the recent years, nanotechnology has drawn the attention of many researchers to develop innovative solutions to satisfy the growing demand in hydrocarbons. The potential application of nanoparticle dispersions has significantly advanced into the upstream oil and gas industry, from drilling, formation characterization, to improved hydrocarbon and geothermal heat recovery (Mokhatab et al. 2006). The success of all of the petroleum engineering applications rests on the transport of nanoparticles in wellbores and in

hydrocarbon formations. The mobility of nanoparticle in natural formations is strongly influenced by the dispersion stability of nanoparticles in a continuous phase. Typical subsurface conditions such as temperature, pH, and electrolyte concentration vary over wide ranges. It is thus difficult to control the stability of nanoparticle dispersion under reservoir conditions, particularly at high salinity and high temperature.

Silica,  $\text{SiO}_2$ , dispersions have been of interest in colloidal science because of their many applications and because their anomalous behavior of aggregation may not be predicted by Derjaguin–Landau–Verwey–Overbeek (DLVO) theory (Derjaguin and Landau 1941; Verwey and Overbeek 1948) (Healy 2006). An aqueous nanoparticle dispersion is defined to be stable when the number of particles in a unit volume is constant with respect to time (Kissa 1999). The stability of silica dispersions depends on the structure of the silica surfaces and associated water molecules that define the characteristics of the near surface region (Hofmann et al. 1934; Zhuravlev 1987; Yalamanchili et al. 1996; Asay and Kim 2005; Hair 2006). The presence of silanol groups ( $\text{Si}(\text{OH})$ ) on a silica surface was postulated by Hofmann in 1934. These hydrophilic silanol groups on a silica surface act as binding sites ( $\text{H}^+$  bonds) for water. From experimental observations with silica gels, aerosil-gels, and porous glasses, Zhuravlev (1987) concluded that a silanol group was the most probable compound on the surface of amorphous, fully hydroxylated silica, and that one OH group corresponded to one surface Si atom. The protonation and deprotonation of these silanol groups determine the surface charge of silica nanoparticles and the extent of the repulsive energy to keep them dispersed in the solution. For a given surface charge, the aggregation of silica nanoparticles occurs because of the presence of electrolytes. The increasing rate of aggregation of silica nanoparticles with concentration of electrolytes is known but not well understood (Roberts 2006). The interparticle interactions of two silica nanoparticles have been recently investigated through molecular simulations to understand the stability of dispersion (Jenkins et al. 2007, 2008; Lane et al. 2009). Jenkins et al. (2007, 2008) have shown that the electrical surface charge of silica nanoparticle in the presence of background sodium,  $\text{Na}^+$ , concentration affects the ordering of water molecules around the silica surface

and the particle–water interactions (oscillatory interparticle forces). Lane et al. (2009) studied the forces acting on surface-coated silica nanoparticles and concluded that surface coating suppressed the force oscillations. The study of the effects of pH, temperature, cation type, and electrolyte concentration on the stability of silica nanoparticle dispersions is yet to be explored.

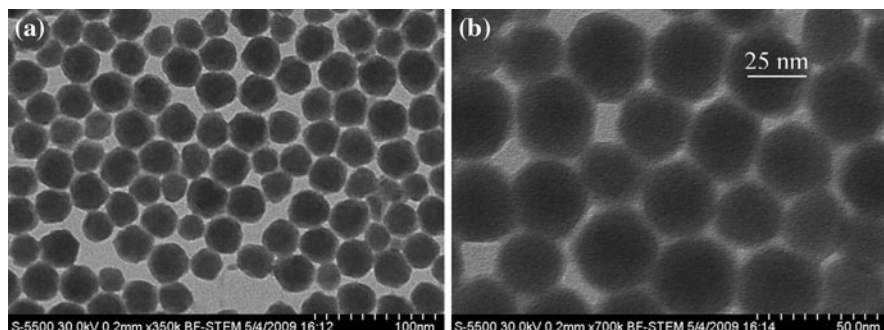
In this article, we present a systematic study of the stability of silica nanoparticle dispersions. The effect of pH on the colloidal stability of silica is determined by different analytical methods. We identify a critical salt concentration (CSC) for monovalent ( $\text{NaCl}$ ) and divalent cations ( $\text{CaCl}_2$ ,  $\text{MgCl}_2$ , and  $\text{BaCl}_2$ ) above which silica nanoparticle dispersion becomes unstable. Development of quantitative methods for determining the CSC is discussed. The effect of temperature on the CSC is also investigated.

## Materials and methods

The material under study is an aqueous dispersion of silica particles that have a mean diameter of 25 nm and an unmodified (bare) surface. The shape and size of silica particles were examined by a Hitachi-S5500 scanning transmission electron microscope (STEM). We dried a droplet of the silica nanoparticle dispersion on a commercial copper transmission electron microscope (TEM) grid with carbon film support. The images of silica nanoparticles are in Fig. 1 at two magnifications. The result from dynamic light scattering (DLS) measurements also shows a mean diameter of 25 nm with a polydispersity index of 0.077 indicating a narrow size distribution. The shape of the silica nanoparticles is angular rather than spherical. Iler (1971) argued that the capillary forces during drying do not affect the shape of particles. Van Blaaderen and Vrij (2006) observed that drying does not influence the radius of particles determined with TEM measurements and that the shape of silica particles depends mainly on the method of synthesis.

A stock solution containing 41.13% by weight silica nanoparticles was diluted with deionized water up to a desired silica concentration. Then, we adjusted the pH of the silica dispersion samples by adding a diluted hydrochloric acid (HCl) solution.  $\text{NaCl}$ ,  $\text{MgCl}_2$ ,  $\text{BaCl}_2$ , and  $\text{CaCl}_2$  were the inorganic salts that we used in the experiments about the effects

**Fig. 1** The bright field scanning transmission electron microscopy (STEM) images of dried silica dispersions at **a** 350 k magnification and **b** 700 k magnification



of electrolytes on aqueous dispersion stability. All the chemicals were of analytical grade quality. We mixed the stock solutions of the inorganic salts and the silica dispersion samples to reach the desired electrolyte concentrations. We used typical ranges of salinity and hardness from natural hydrocarbon reservoir brines in our experiments.

A spectrum 100 FTIR spectrometer made by Perkin Elmer was used to identify chemical functional groups present in the silica nanoparticles and their dispersions. Samples were positioned in direct contact with an attenuated total reflectance (ATR-FTIR) diamond crystal. The ATR-FTIR spectra were then recorded from 4000 to 600 cm<sup>-1</sup> at a resolution of 2 cm<sup>-1</sup>. A baseline correction was applied to ATR-FTIR spectra before each measurement.

We also used a Cary 50 ultraviolet-visible spectrophotometer (UV-vis) to analyze optical absorbance of silica dispersions. The absorbance–time relationship provided a means to study the aggregation of silica dispersions.

We used a zeta potential analyzer (Zeta Plus) with a DLS option from Brookhaven Instruments Corporation to determine the zeta potential and effective particle diameter of silica nanoparticle dispersions.

## Results and discussion

### The effect of pH on aqueous stability of silica nanoparticle dispersion

Figure 2 shows the respective ATR-FTIR transmittance spectra of deionized water, a dry silica sample, and a silica dispersion sample with a pH of 9.65 after dilution of stock solution to 1 wt% silica. The dry silica sample was prepared by evaporating water from

the silica dispersion at 120 °C for 12 h. Deionized water shows a broad peak at 3330 cm<sup>-1</sup> and a sharp peak at 1629 cm<sup>-1</sup> because of the stretching and bending vibrations of the O–H bonds in the water molecules. Comparing the spectra of deionized water and the silica dispersion reveals the presence of silica nanoparticles by a characteristic Si–O peak at 1100 cm<sup>-1</sup>. The deionized water curve coincided with the silica dispersion at the peaks corresponding to vibrations of O–H bonds. In the spectrum of the silica powder, two peaks corresponding to Si–O bond vibration occur at 793.4 and 1055.3 cm<sup>-1</sup>. Morrow and Molapo (2006) also observed similar peaks at 1100 and 800 cm<sup>-1</sup> for a silica thin film. A small and broad peak at 3300 cm<sup>-1</sup> and a small peak at 1650 cm<sup>-1</sup> in the spectrum of the silica powder indicate the presence of adsorbed water that remains after drying. The transmittance corresponding to the Si–O peak at 1100 cm<sup>-1</sup> in the silica dispersion is large compared to silica powder because of the small concentration of silica nanoparticles (1 wt%) in the dispersion. For a given nanoparticle concentration, the area of the Si–O peak varies with the degree of hydroxylation of silica nanoparticle surface as pH changes. Moreover, the Si–O peak at 793.4 cm<sup>-1</sup> observed with powder silica particles is suppressed by water in silica dispersions (Fig. 2). Therefore, only the Si–O peak at 1100 cm<sup>-1</sup> is used to evaluate the effect of pH on the aqueous stability of silica nanoparticle dispersion.

We measured the infrared light (IR) transmittance of two respective series of 0.5 and 1 wt% silica particle dispersions, whose pH varied over a wide range from 2.5 to 10. All of these samples exhibit a stable clear phase, indicating an indiscernible effect of pH on the stability of silica nanoparticle dispersion. However, a plot of Si–O peak area, which is the

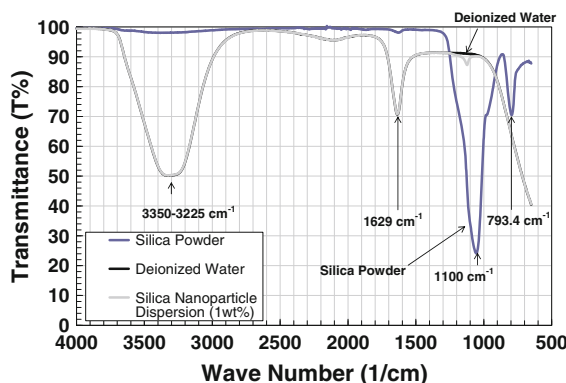


**Fig. 2** ATR-FTIR transmission spectrum of dried silica powder, 25-nm silica particle dispersion, and deionized water. Stretching and bending vibrations of water molecules show peaks at 3330 and 1629  $\text{cm}^{-1}$ , respectively. The silica powder has the Si–O bond vibrations at 793.4 and 1055.3  $\text{cm}^{-1}$ . Only the Si–O at 1100  $\text{cm}^{-1}$  is detectable in case of silica dispersion

area under the peak at 1100  $\text{cm}^{-1}$ , versus pH, as shown in Fig. 3, suggests a significant variation of silica nanoparticle surface structure with pH. The peak area first decreases sharply as pH increases, and then levels off at around a pH = 7, regardless of particle concentration. A small increase in the peak area at a given pH is because of an increase in particle concentration.

The surface charge of metal-oxide particles in water may vary from positive to negative as pH increases because of surface deprotonation (Hunter 2001). The isoelectric point (IEP) is defined as the pH

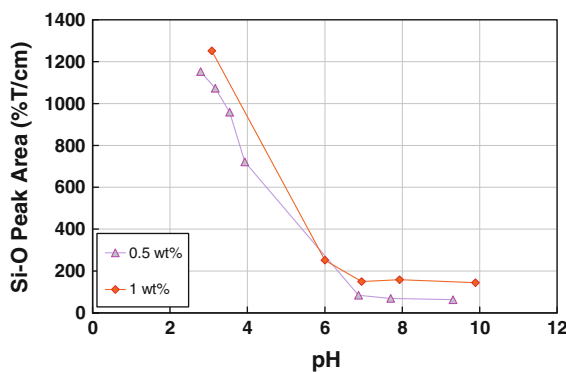


**Fig. 3** The area under the Si–O peak at 1100  $\text{cm}^{-1}$  as a function of pH for 0.5 and 1 wt% particle concentrations. The change in the slope of the peak area of the Si–O bond around pH = 7 indicates a structural change of silica nanoparticle surface

at which the surface is neutrally charged. The measured zeta potential, which represents the potential at the shear plane (Hunter 2001) of the silica nanoparticles, is plotted versus pH as shown in Fig. 4. It is around  $-45$  mV as pH decreases from 10 to 6, but sharply increases with further decrease in pH. This trend is observed for both 0.5 and 1 wt% particle concentrations, which is consistent with the relationship between IR transmittance and pH (see Fig. 3). Furthermore, extrapolating the potential curve to the smaller pH range in Fig. 4 suggests that the silica surface approaches the IEP at a pH around 3.4.

The pH-induced aggregation of silica particles is not seen by visual observation because of the possible nanometer-sized aggregates. Another way to identify the presence of nanoparticle aggregation is through UV-vis spectroscopy and DLS. Figure 5a shows the light absorbance of silica dispersions as a function of pH for two different particle concentrations at 400 nm. The variation of absorbance with pH could be clearly observed at this wavelength. From this figure, the absorbance does not significantly change with pH. This evidences the absence of particle aggregation, which is confirmed by the results from the DLS measurements in Fig. 5b. The effective particle diameter increases by a factor of 1.36 as pH decreases from 10 to 2. Therefore, particle aggregation is not responsible for the observed slight change of the effective particle diameter with pH despite of

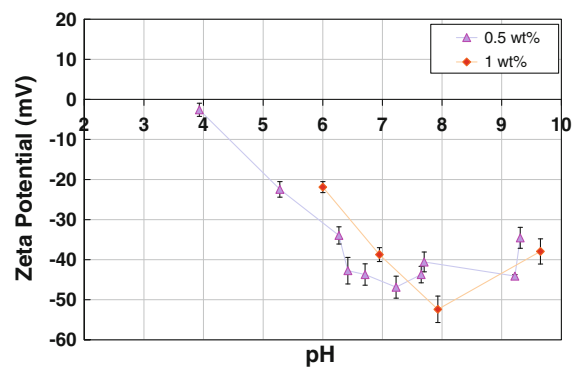


**Fig. 4** Zeta potential of silica particle dispersions as a function of dispersion pH. The vertical error bars in the graph are the mean standard errors of the zeta potential measurements. The IEP is estimated as pH = 3.4 by extrapolation of linear regression fit to points at pH = 8 or smaller. The zeta potential measurements below pH = 4 exceeded the conductance limit of the zeta potential analyzer; therefore, zeta potential measurements are not in this pH range

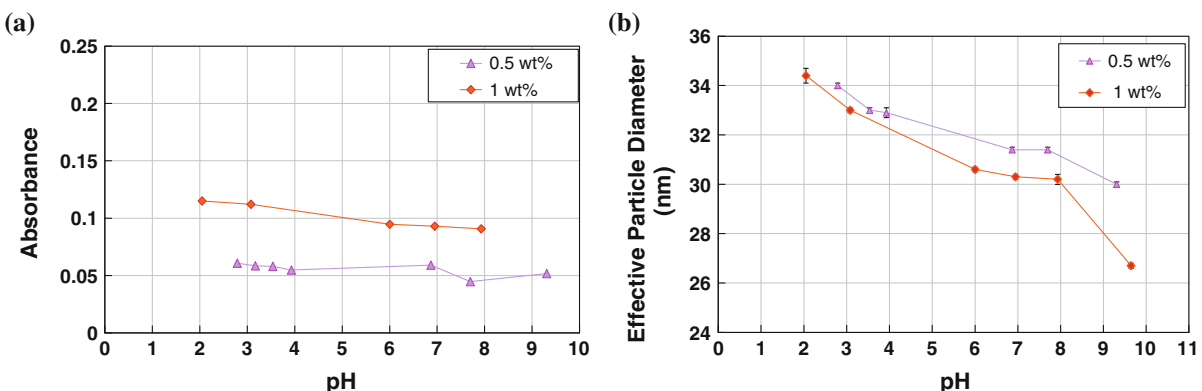


**Fig. 5** **a** UV-vis absorbance of 0.5 and 1 wt% silica particle dispersions at 400-nm wave length as a function of pH. **b** The effect of pH on effective particle diameter for 0.5 and 1 wt% silica dispersions by DLS measurements

the significant pH-induced reduction of particle surface charge (see Fig. 4). The effective diameter determined by DLS is the diameter of the nanoparticle plus the thickness of a layer of water and ions that are bound, with varying degrees of strength, to the particle. The latter is partially determined by the surface potential of particles, which is in turn influenced by pH as shown in Fig. 4. This most likely explains the relationship between the effective particle diameter and pH shown in Fig. 5b.

The silica nanoparticles used in the experiments on the effect of pH made a stable clear phase with water. The effective particle diameter was close to the actual diameter of nanoparticles (Fig. 5b). These clear dispersions had absolute zeta potentials much smaller than 40 mV, which indicates the degree of the stability of dispersion (ASTM Standard 1985). When the extent of the repulsive energy is smaller compared to the van der Waals attraction energy, the dispersion becomes unstable giving rise to the aggregation of particles. As discussed above, the silica nanoparticles exhibit a stable dispersion in the pH range studied. Kitchener (1971) drew attention to this anomalous stability of silica dispersions, in contradiction with DLVO theory (Derjaguin and Landau 1941; Verwey and Overbeek 1948), around pH 2–3 where their zeta potential is minimal. Kitchener (1971) discussed that the existence of polysilicic acid filaments on the silica surface formed *in situ* could be the reason for this extraordinary stability around the IEP.

These thin silica hairs on the surface (Iler 1971) could push the double layer repulsion out to extend further than van der Waals attraction and also

generate an additional short-range steric repulsion (Israelachvili and Wennerstrom 1996).

#### Phase behavior of silica nanoparticle dispersions in the presence of electrolytes

Electrolytes could also destabilize particle dispersions by compressing the electrical double layer. As the electrolyte concentration increases, the energy barrier is lowered to an extent that kinetic energy of particles dictates the kinetics of particle aggregation (Derjaguin and Landau 1941; Verwey and Overbeek 1948). In this section, the effect of NaCl as an indifferent electrolyte on the stability of silica nanoparticle dispersions is evaluated. The NaCl is indifferent because it does not adsorb on the particles.

Figure 6 shows the phase behavior of silica dispersions that are different in NaCl and particle concentrations. For small particle concentration (e.g., 0.5 wt% particle in Fig. 6), the addition of NaCl up to around 1.5 wt% does not destabilize the aqueous dispersion of silica nanoparticles. However, a further increase in NaCl concentration leads to a phase transition. This phase behavior suggests that 1.5 wt% NaCl represents a CSC above which particle aggregation and sedimentation visually occurs. When the NaCl concentration is increased above its CSC, three distinct subsequent stages of particle aggregation could be observed: (1) an early time stage characterized with a single clear phase (e.g., vials shown in Fig. 6 with 0.5 wt% particle concentration and 3 wt% NaCl at 1 h), (2) a precipitation stage with a single turbid phase (e.g., same vials at 10 days later), and (3)

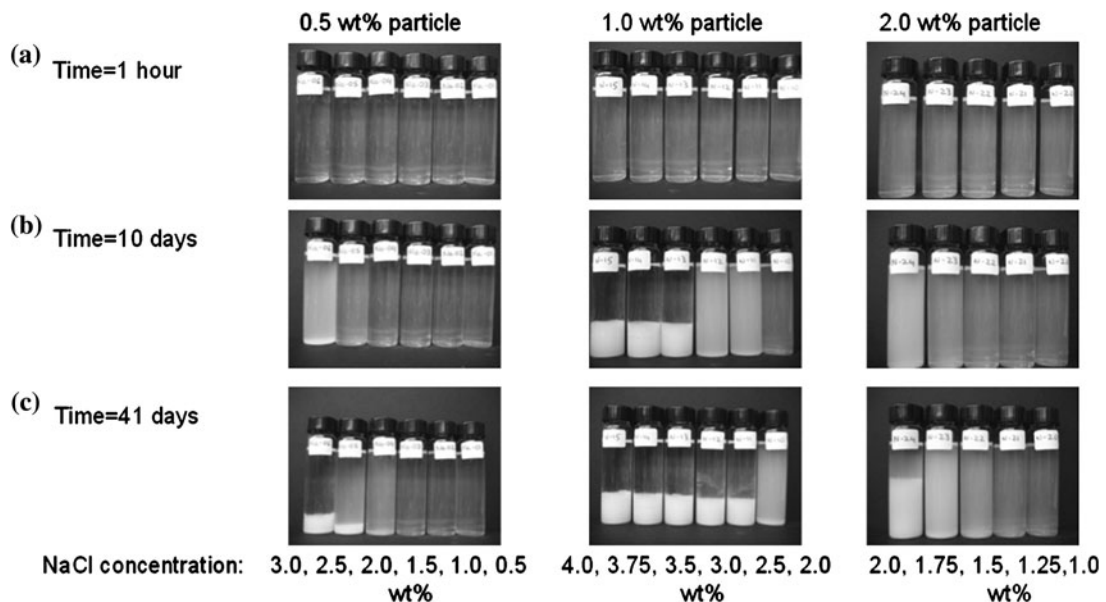


**Fig. 6** Photographs of sealed tubes that show the phase behavior of silica nanoparticle dispersions at various NaCl and nanoparticle concentrations at **a** 1 h, **b** 10 days, and

**c** 41 days. Three distinct sequential stages of aggregation, i.e., single clear phase, a turbid single phase, and two separate phases

a sedimentation stage with two separate phases (e.g., the same vials after 41 days). The subsequent occurrence of the precipitation and sedimentation stages is accelerated by either increasing NaCl or particle concentration. For example, Fig. 6 shows that for 2 wt% NaCl concentration the particle dispersion with 2 wt% particle concentration approaches the end of the precipitation stage after 10 days while the dispersion with 0.5 wt% particle concentration is still in the early time stage. However, these two factors were found not to significantly influence the CSC for NaCl.

Particle aggregation occurs during the early time stage when the electrolyte concentration is above its CSC. However, the formation of nanometer-sized aggregates may not be visually observed. In addition, a CSC could be determined accurately through DLS measurements of effective particle diameter. It is important to determine the light absorption characteristic of silica particle aggregates in the UV-vis range as the UV-vis spectrophotometer provides a convenient technique for studying aggregation kinetics. For the above purposes, DLS and UV-vis measurements were conducted on a series of particle dispersions with different electrolyte concentrations. The results are in Fig. 7.

Figure 7 shows that the absorbance profile for 0.5 wt% particle concentration at 400-nm wavelength is characterized by a transition from a uniform to a sharp increase as NaCl increases above the critical value. This critical value does change with time (i.e., from 2 wt% at 1 h to 1 wt% after 43 days) and eventually reaches an approximate value of 1 wt%, which defines the equilibrium CSC for NaCl. The

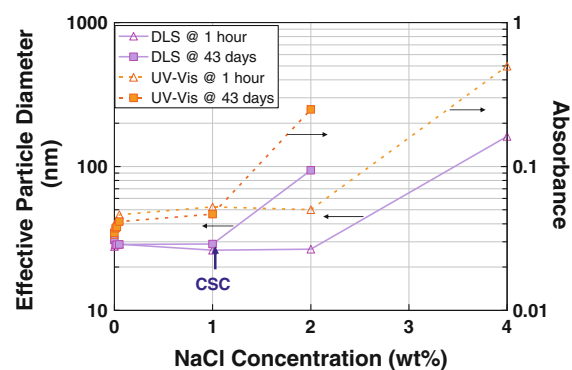


**Fig. 7** Effective particle diameter and UV-vis absorption at 400-nm wave length of 0.5 wt% silica dispersions in the presence of NaCl. A significant increase in effective diameter and absorbance occurs initially at 2 wt% NaCl, but this critical concentration shifts to an equilibrium value (CSC) of 1 wt% at 43 days

variations of effective particle diameter in time and with NaCl concentration are in Fig. 7. The effective particle size increases sharply from 25 to 200 nm with NaCl concentration above CSC. The effective particle diameter profiles are very close to the UV-vis light absorbance profiles. Both techniques give almost the same CSC. Therefore, the UV-vis spectrometry is also used in determining the kinetics of particle aggregation.

Figure 8 shows the light absorbance for 0.5 wt% particle dispersion in the presence of 3 wt% NaCl (above the NaCl CSC). The rate of increase in absorbance reflects the kinetics of particle precipitation. In the sedimentation stage, the gravitational potential overcomes the dispersive interparticle and particle–solvent interactions. The sedimentation of nanoparticles was clearly observed after around 190 h. Plaza et al. (2002) carried out stability experiments with hematite/yttrium oxide core–shell particles by measuring their optical absorbance. They suggested that the slope of an absorbance curve carries the most significant information about particle–particle aggregation. A positive slope indicates a doublet of particles that has larger extinction cross section than two individual particles sufficiently far apart. In our experiments with 1, 2, and 3 wt% NaCl at 0.5 wt% silica concentration, we observed a negative slope during the early time stage (i.e., first 1 h) which may indicate that a doublet of silica particles has a smaller extinction cross section than two individual particles far apart in the dispersion (Plaza et al. 2002). This negative slope is not visible in Fig. 8 because of the large time scale.

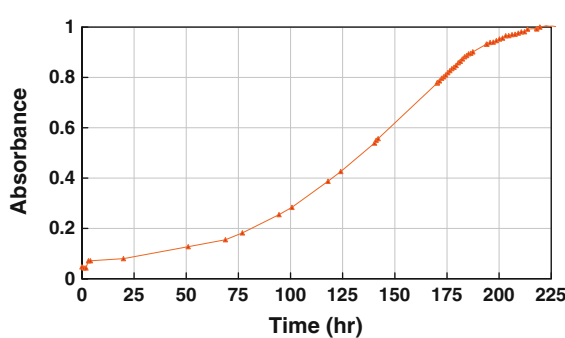


**Fig. 8** UV-vis light absorption of a 0.5 wt% silica particle dispersion with 3 wt% NaCl as a function of time

#### Effect of divalent cations on critical salt concentration

Figures 9 and 10 show phase behavior images of silica particle dispersions in the presence of MgCl<sub>2</sub> and CaCl<sub>2</sub>, respectively. There was no background NaCl in these experiments. For both Mg<sup>2+</sup> and Ca<sup>2+</sup>, an increase in concentration above a critical value gives rise to particle aggregation, in consistence with the phase behavior for NaCl (see Fig. 6). A silica particle dispersion exhibits an equilibrium clear phase for divalent cation concentration lower than 0.02 wt%, which is 100 times lower than that for the monovalent cation (CSC for NaCl is 1 wt%). For a divalent cation concentration above 0.04 wt%, the particle aggregation is so effective that the early time stage is almost absent; sedimentation begins only after 1 day. Among these cations, Mg<sup>2+</sup> exhibits the most capability of particle dispersion destabilization. Furthermore, comparing phase transition by Mg<sup>2+</sup> (Fig. 9) and Ca<sup>2+</sup> (Fig. 10) at a given electrolyte and particle concentrations reveals that an increase in particle concentration accelerates aggregation for divalent cations. An increase in nanoparticle concentration shortens the average distance travelled by a particle between collisions, resulting in an increase in aggregation rate for a salt concentration above CSC. However, the particle concentration does not influence the CSCs for these cations. Elimelech et al. (1998) argue that particle concentration should not affect critical coagulation concentration if the electrolyte is indifferent. In other words, if there is not any specific adsorption of counterions onto the surface of a particle, then the extent of the repulsive energy is not changed and hence the concentration of particles does not affect CSC.

Figure 11 shows the absorbance at 400-nm wavelength as a function of concentration of the chloride salts for Mg<sup>2+</sup>, Ca<sup>2+</sup>, and Ba<sup>2+</sup> for 1 wt% particle concentration. The CSCs, determined at a point of sharp change in the UV-vis absorbance profiles in Fig. 11, are 0.0125 wt% for MgCl<sub>2</sub> and 0.025 wt% for both CaCl<sub>2</sub> and BaCl<sub>2</sub>. These values are confirmed by the measured effective particle diameter as a function of salt concentration as in Fig. 12. From this figure, the aggregate size is much more sensitive to the addition of divalent than monovalent cations.

Colic et al. (1998) studied the influence of monovalent cation size (Li<sup>+</sup>, Na<sup>+</sup>, K<sup>+</sup>, and Cs<sup>+</sup>) on

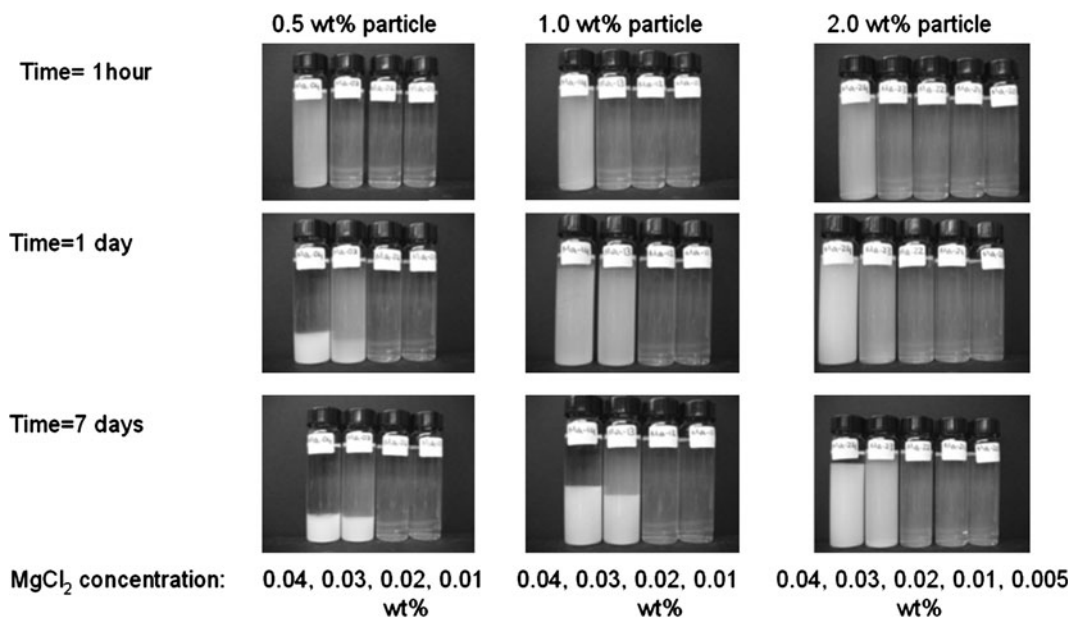


**Fig. 9** Photographs of sealed tubes that illustrate the phase behavior of silica dispersions with MgCl<sub>2</sub> at 1 h, 1 day, and 7 days at 25 °C. Three distinct sequential stages of aggregation are observed at various MgCl<sub>2</sub> and nanoparticle concentrations.

The transition between a stable and an unstable dispersion (aggregation followed by sedimentation) occurs around 0.03 wt% MgCl<sub>2</sub> for all the three nanoparticle concentrations

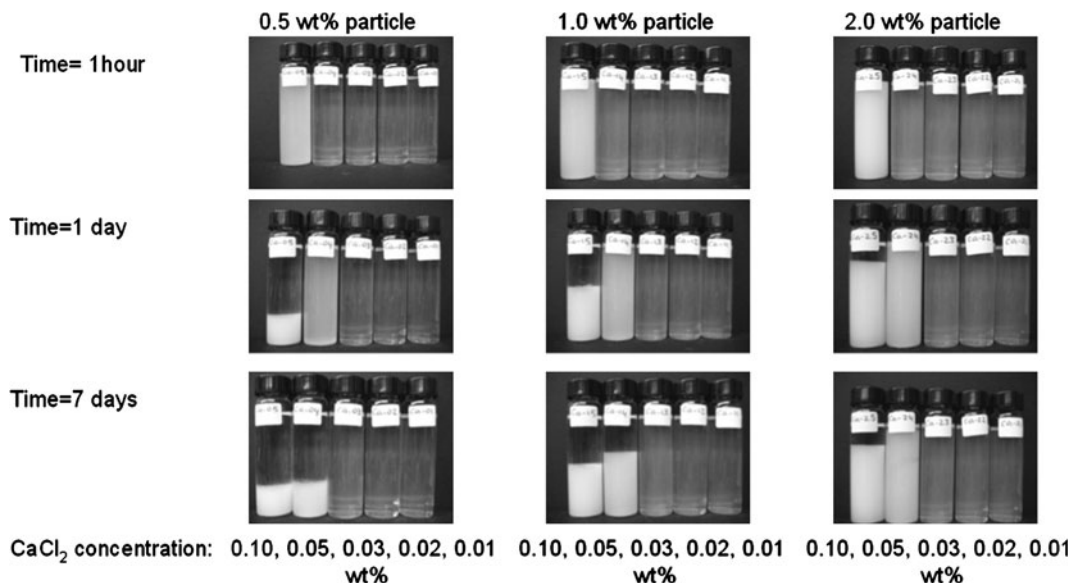


**Fig. 10** Photographs of sealed tubes that illustrate the phase behavior of silica dispersions with CaCl<sub>2</sub> at 1 h, 1 day, and 7 days at 25 °C. Three distinct subsequent stages of aggregation are observed at various CaCl<sub>2</sub> and nanoparticle

concentrations. The transition between a stable and an unstable dispersion (aggregation followed by sedimentation) occurs around 0.05 wt% CaCl<sub>2</sub> for all the three nanoparticle concentrations

short range repulsive forces in silica slurries at large salt concentrations. The authors argued that the layer of structured water molecules around the silica

particle's surface favors the accommodation of small ions that prefer to be surrounded by organized water at pH greater than IEP. Hence, smaller cations can

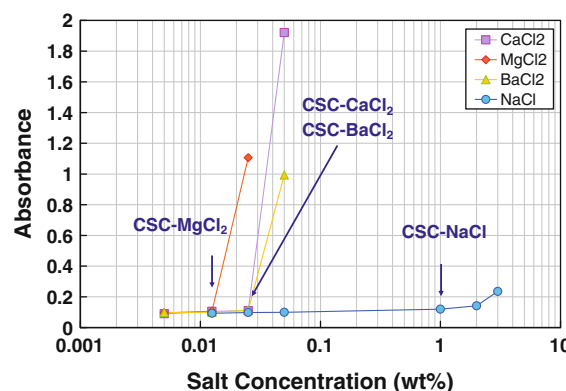


**Fig. 11** UV-vis absorbance of a 1 wt% silica dispersion in the presence of different salts (NaCl, MgCl<sub>2</sub>, CaCl<sub>2</sub>, and BaCl<sub>2</sub>) at 400-nm wavelength at 25 °C. Mg<sup>2+</sup> exhibits the smallest CSC while the CSCs for Ca<sup>2+</sup> and Ba<sup>2+</sup> are both about 0.025 wt%

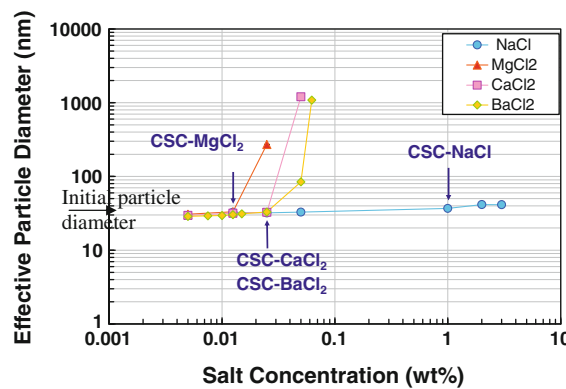


**Fig. 12** Effective particle diameters for 1 wt% silica dispersion as a function of NaCl, MgCl<sub>2</sub>, CaCl<sub>2</sub>, and BaCl<sub>2</sub> concentrations at 25 °C. An increase in the effective diameter indicates aggregation of the silica particles

penetrate deep into the water layer at the particle surface resulting in less repulsive force compared to larger ions that reside outside the hydration layer (Torrie et al. 1989). The mechanism for the short-range repulsion would be the collapse of the counterion cloud. Our observations on the stability of silica dispersions with divalent cations Mg<sup>2+</sup>, Ca<sup>2+</sup>, and Ba<sup>2+</sup> agree with this theory. Mg<sup>2+</sup> being the smallest cation with highest affinity to water induces the smallest repulsive force and, hence, exhibits the least CSC compared to Ca<sup>2+</sup> and Ba<sup>2+</sup>.

The significant difference in CSC between the monovalent and divalent cations could be further explained by the DLVO theory (Derjaguin and Landau 1941; Verwey and Overbeek 1948). The interaction

potential between two spherical nanoparticles includes the attraction ( $V_A$ ) and repulsion energies ( $V_R$ ) as described by Eqs. 1 and 2, respectively

$$V_A = -\frac{A}{12} \left( \frac{1}{x^2 - 1} + \frac{1}{x^2} + 2 \ln \left( 1 - \frac{1}{x^2} \right) \right) \quad (1)$$

$$V_R = 2\pi\epsilon_0\epsilon_r a^2 \zeta^2 \ln [1 + \exp(-2\kappa a (x - 1))] \quad (2)$$

$$V_T = V_A + V_R \quad (3)$$

where  $x$  is the ratio of the center-to-center distance of spheres,  $r$ , to the diameter of the sphere,  $2a$ ;  $\kappa$  is the inverse of Debye length;  $\epsilon_0\epsilon_r$  is the dielectric permittivity; and  $A$  is the Hamaker constant. For silica dispersion, the calculated value of  $A$  is  $6.02 \times 10^{-21}$  J in agreement with previously proposed constants for silica (Franks 2002; Dumont 2006). The diffuse layer potential,  $\zeta$ , is obtained from zeta potential measurements. Equation 2 shows that the magnitude of the repulsive energy depends on the Debye length, which decreases with increasing electrolyte concentration. In Eq. 3,  $V_T$  is the total interaction energy.

Figure 13 presents the normalized interaction energy ( $V_T/kT$ ) between two identical spheres as a function of dimensionless distance  $x$ . Here,  $k$  is the Boltzmann constant, and  $T$  the temperature. A secondary minimum in energy occurs at NaCl concentrations greater than 1 wt% (Fig. 13b). In Fig. 14, we present the area under the DLVO curve as a function of electrolyte concentration. This figure also shows the relationship between electrolyte concentration and the amount of energy ( $V_T/kT$ ) required to bring two nanoparticles from infinity to a critical distance,  $x_c$ , that is shorter than that at which particle aggregation is highly promoted because of the increasing attraction energy as  $x$  decreases. The gradient of the interaction potential with respect to  $x$  becomes positive for  $x$  which is smaller than  $x_c$ . The integration term, the area under the DLVO curve, decreases first sharply then much more gradually as electrolyte concentration increases, Fig. 14a and b. This gradually decreasing slope, in the region between 0.5 and 1.5 wt% NaCl in Fig. 14a, is the region where the transition of a stable dispersion into an unstable state occurs. The range of electrolyte concentration for this transition region is significantly reduced as the cation's valence increases and is consistent with the measured CSCs for Na<sup>+</sup>, Ca<sup>2+</sup>, and Mg<sup>2+</sup>.

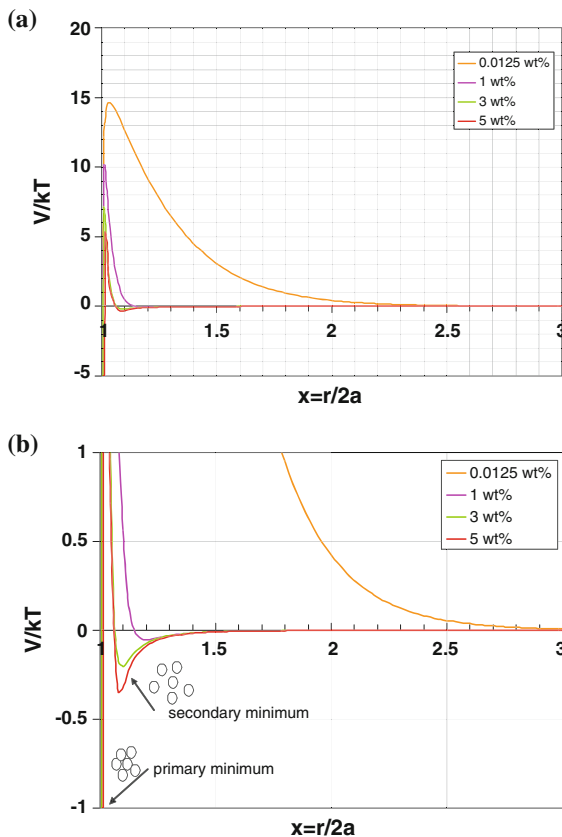


**Fig. 13** Two-particle interaction potential as a function of dimensionless separation distance according to DLVO theory for **a** NaCl concentrations. The secondary and primary minima are shown clearly in the **b** small scale range of the y-axis, a zoom-in of (a)

#### Effect of temperature on critical salt concentration

To investigate the effect of temperature on the CSC, we used DLS to measure particle size on a series of 1 wt% silica dispersions with different salt types (NaCl, CaCl<sub>2</sub>, and MgCl<sub>2</sub>) and concentrations at 25 and 70 °C. The results, shown in Fig. 15, indicate that the CSC is significantly reduced as temperature increases. This observation may be explained based on relative magnitude of the energy barrier and the average kinetic energy of nanoparticles as shown in Figs. 13 and 14. An increase of the average kinetic energy with temperature gives rise to the particle collisions that result in aggregation. As a consequence, a higher energy barrier (i.e., lower salt concentration) is required to maintain the aqueous stability of nanoparticle dispersion.

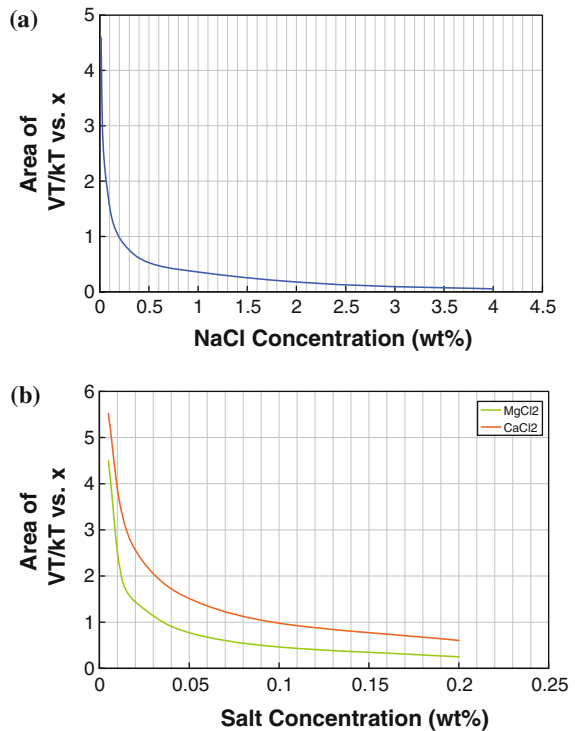


**Fig. 14** Relationship between electrolyte concentration and the amount of energy ( $V_T/kT$ ) required to bring two nanoparticles from infinity to a critical distance,  $x_c$ , for **a** NaCl and **b** CaCl<sub>2</sub> and MgCl<sub>2</sub> concentrations

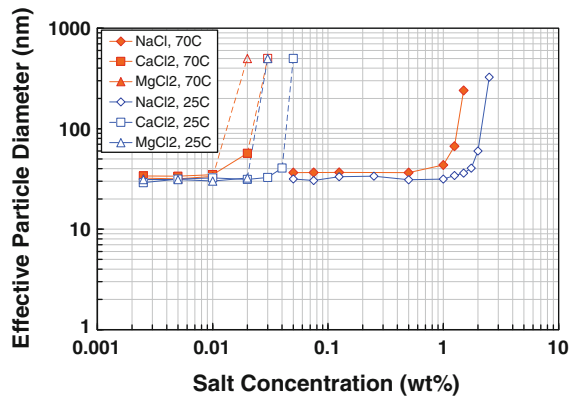


**Fig. 15** DLS measurements of 1 wt% silica dispersion in the presence of different salts (NaCl, CaCl<sub>2</sub>, and MgCl<sub>2</sub>) at 25 and 70 °C. DLS measurements are taken after 18 days

#### Conclusions

We studied the stability of silica particles of 25-nm diameter in aqueous solutions under changing pH, salt concentration (NaCl, MgCl<sub>2</sub>, CaCl<sub>2</sub>, and BaCl<sub>2</sub>),

and temperature using ATR-FTIR, UV-vis spectrophotometry, DLS, and a zeta potential analyzer. Spectral analysis of the Si–O bond at 1110 cm<sup>-1</sup> with the ATR-FTIR indicates a structural change on the surface of silica particles because of the change in the pH of the solution, which agrees with zeta potential results. Changing the pH does not affect the aggregation in the absence of electrolyte for the range of pH studied. However, the addition of different types of salts (NaCl, CaCl<sub>2</sub>, MgCl<sub>2</sub>, and BaCl<sub>2</sub>) causes aggregation of the silica nanoparticles.

We observed a CSC for a given electrolyte below which the silica nanoparticles are well dispersed in an aqueous phase and above which flocculation of silica nanoparticles occur and the aggregates settle by gravity. The CSC depends on electrolyte type, but is not influenced by silica nanoparticle concentration.

Divalent cations Mg<sup>2+</sup>, Ca<sup>2+</sup>, and Ba<sup>2+</sup> are more effective in destabilizing (i.e., causing aggregation) the nanoparticle dispersion than the monovalent cation Na<sup>+</sup>. The CSC for Na<sup>+</sup> is about 100 times larger than that of divalent cations. Among these divalent cations, Mg<sup>2+</sup> is the most effective in aggregating the silica particles. The presence of the CSC for the electrolytes studied in this study could be explained by the DLVO theory.

An increase in temperature from 25 to 70 °C increases the aggregation rate, and hence lowers the CSC. The reduction in CSC is more significant for monovalent cation Na<sup>+</sup> than it is for divalent cations Mg<sup>2+</sup> and Ca<sup>2+</sup>. This suggests that the effect of cation valance is dominant over the effect of thermal energy within the range of temperature used in this study.

**Acknowledgment** This study is supported by the Advanced Energy Consortium (AEC), through the contract BEG08-020. We would like to thank 3M company, particularly Dr. Jimmie Baran for providing the nanoparticles and for scientific discussions. We would also like to acknowledge great help from Dr. Sujewa Palayangoda and Ms. Wenjun Liu for their great contributions to the experiments.

## References

- Asay DB, Kim SH (2005) Evolution of the adsorbed water layer structure on silicon oxide at room temperature. *J Phys Chem B* 109:16760–16763
- ASTM Standard D 4187-82, Zeta Potential of Colloids in Water and Waste Water, 1985
- Colic M, Fisher ML, Franks GV (1998) Influence of ion size on short-range repulsive forces between silica surfaces. *Langmuir* 14:6107–6112
- Derjaguin BV, Landau L (1941) Theory of the stability of strongly charged lyophobic sols and the adhesion of strongly charged particles in solutions of electrolytes. *Acta Physicochim USSR* 14:633–662
- Dumont F (2006) Stability of sols: do the silica hydrosols obey the DLVO theory? In: Bergna HE, Roberts WO (eds) *Colloidal silica: fundamentals and applications*. CRC Press, Boca Raton, pp 243–245
- Elimelech M, Gregory J, Jia X, Williams RA (1998) Particle deposition and aggregation: measurement modelling and simulation. Butterworth-Heinemann, Woburn
- Franks GV (2002) Zeta potentials and yield stresses of silica suspensions in concentrated monovalent electrolytes: isoelectric point shift and additional attraction. *J Colloid Interface Sci* 249:44–51
- Hair ML (2006) Surface chemistry of silica. In: Bergna HE, Roberts WO (eds) *Colloidal silica: fundamentals and applications*. CRC Press, Boca Raton, pp 257–260
- Healy TW (2006) Stability of aqueous silica sols. In: Bergna HE, Roberts WO (eds) *Colloidal silica: fundamentals and applications*. CRC Press, Boca Raton, pp 247–252
- Hofmann U, Endell K, Wilm D (1934) Röntgeno-graphische und kolloidchemische Untersuchungen über Ton. *Angew Chem* 47:539–558
- Hunter RJ (2001) Foundations of colloid science. Oxford University Press, New York
- Iler RK (1971) The chemistry of silica. Wiley, New York
- Israelachvili J, Wennerstrom H (1996) Role of hydration and water structure in biological and colloidal interactions. *Nature* 379:219–225
- Jenkins S, Kirk SR, Persson M, Carlen J, Abbas Z (2007) Molecular dynamics simulation of nanocolloidal amorphous silica particles: part I. *J Chem Phys* 127:224711–1–224711–10
- Jenkins S, Kirk SR, Persson M, Carlen J, Abbas Z (2008) Molecular dynamics simulation of nanocolloidal amorphous silica particles: part II. *J Chem Phys* 128:164711–1–164711–10
- Kissa E (1999) *Dispersions: characterizations testing, and measurement*. Marcel Dekker, New York
- Kitchener JA (1971) General discussion. *Faraday Disc* 52: 372–380
- Lane JMD, Ismail AE, Chandross M, Lorenz CD, Grest GS (2009) Forces between functionalized silica nanoparticles in solution. *Phys Rev E* 79:050501
- Mokhatab S, Fresky MA, Islam MR (2006) Applications of nanotechnology in oil and gas E&P. *J Pet Technol Online* 58:4
- Morrow BA, Molapo DT (2006) Infrared studies of chemically modified silica. In: Bergna HE, Roberts WO (eds) *Colloidal silica: fundamentals and applications*. CRC Press, Boca Raton, pp 287–294
- Plaza RC, Quirantes A, Delgado AV (2002) Stability of dispersions of colloidal hematite/yttrium oxide core–shell particles. *J Colloid Interface Sci* 252:102–108
- Roberts WO (2006) Manufacturing and applications of waterborne colloidal silica. In: Bergna HE, Roberts WO

- (eds) Colloidal silica: fundamentals and applications. CRC Press, Boca Raton, pp 131–176
- Torrie GM, Kusalik PG, Patey GN (1989) Theory of the electrical double layer: ion size effects in a molecular solvent. *J Chem Phys* 91:6367–6375
- Van Blaarderen A, Vrij A (2006) Synthesis and characterization of colloidal model particles made from organoalkoxysilane. In: Bergna HE, Roberts WO (eds) Colloidal silica: fundamentals and applications. CRC Press, Boca Raton, pp 65–80
- Verwey EJW, Overbeek JThG (1948) Theory of stability of lyophobic colloids. Elsevier, Amsterdam
- Yalamanchili MR, Atia AA, Miller JD (1996) Analysis of interfacial water at a hydrophilic silicon surface by *in situ* FTIR/internal reflection spectroscopy. *Langmuir* 12: 4176–4184
- Zhuravlev LT (1987) Concentration of hydroxyl groups on the surface of amorphous silicas. *Langmuir* 3:316–318